University of Groningen

Current Blockades of Proteins Inside Nanopores for Real-Time Metabolome Analysis

Zernia, Sarah; van der Heide, Nieck Jordi; Galenkamp, Nicole Stéphanie; Gouridis, Giorgos; Maglia, Giovanni

IMPORTANT NOTE: You are advised to consult the publisher's version (publisher's PDF) if you wish to cite from it. Please check the document version below.

Document Version
Publisher's PDF, also known as Version of record

Link to publication in University of Groningen/UMCG research database

Current Blockades of Proteins inside Nanopores for Real-Time Metabolome Analysis

Sarah Zernia, Nieck Jordy van der Heide, Nicole Stéphanie Galenkamp, Giorgos Gouridis, and Giovanni Maglia*

Cite This: https://dx.doi.org/10.1021/acsnano.9b09434

Read Online

ACCESS | Metrics & More | Article Recommendations | Supporting Information

ABSTRACT: Biological nanopores are emerging as powerful and low-cost sensors for real-time analysis of biological samples. Proteins can be incorporated inside the nanopore, and ligand binding to the protein adaptor yields changes in nanopore conductance. In order to understand the origin of these conductance changes and develop sensors for detecting metabolites, we tested the signal originating from 13 different protein adaptors. We found that the quality of the protein signal depended on both the size and charge of the protein. The engineering of a dipole within the surface of the adaptor reduced the current noise by slowing the protein dynamics within the nanopore. Further, the charge of the ligand and the induced conformational changes of the adaptor defined the conductance changes upon metabolite binding, suggesting that the protein resides in an electrokinetic minimum within the nanopore, the position of which is altered by the ligand. These results represent an important step toward understanding the dynamics of the electrophoretic trapping of proteins inside nanopores and will allow developing next-generation sensors for metabolome analysis.

KEYWORDS: nanopore, cytolysin A, metabolite sensor, substrate-binding protein, electrochemistry
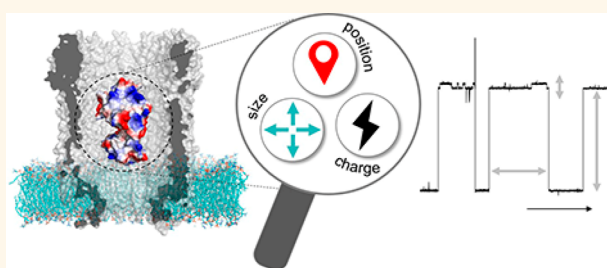
The metabolome is the entirety of all small molecules present in a biological system. These metabolites, which include vitamins, sugars, amino acids, metal ions, and other transmitter molecules,[1] are involved in many essential biological processes.[2] Because the metabolome is influenced by a variety of factors including gene and protein expression,[3,4] as well as lifestyle factors such as diet, age, fitness, hormonal balance, and medication, the metabolome displays the actual health status of an organism[5,6] and is directly related to diseases.[7,8] It is also known that many diseases alter the metabolite composition before developing clinical symptoms.[9] Therefore, the analysis of metabolites in blood, also called blood metabolome, is a promising tool for early stage diagnosis and continuous health-status monitoring. These specifics are crucial for cancer diagnosis and therapy[10] as well as for the evaluation of the progress of dementia[11] or the risk for developing cardiovascular diseases.[12,13]

The diagnosis of diseases by monitoring the blood metabolome requires the targeted detection of hundreds of biomarkers to compare with standard values.[14] The detection of the concentration of multiple biomarkers is important because the fluctuation on individual values can be associated with multiple factors.[15] Today, biomarker detection and

analysis is performed utilizing either mass spectrometry- or NMR-based methods.[16] These techniques are reliable, the sample preparation is kept to a minimum, and high-throughput approaches are possible.[17] However, they require the use of large and complex machines and trained personnel. Therefore, such analytical techniques cannot be incorporated in home-diagnostic devices and are not amenable for real-time analysis. Real-time detection of the blood metabolome using wearable or implantable sensors would be beneficial, as it would allow early and continuous background diagnostics. Indeed, an ideal sensor for metabolite detection should be small, low-powered, selective, and eligible to communicate with silicon-based devices.

Biological nanopores are an emerging class of sensors with such characteristics. A biological nanopore is a protein that forms a water-filled channel on a voltage-clamped hydrophobic

membrane. The output signal is a current of hydrated ions passing through individual nanopores. Crucially, nanopore currents can be easily digitized using small and low-cost devices that contain thousands of individually addressing elements. Most notably, portable devices containing nanopores are now commercially available for DNA sequencing.[18−22] Efforts are underway toward the detection and analysis of peptides[23−26] and proteins,[27−35] as well as the detection of biologically relevant molecules such as amino acids[36−38] or sugars[39] and even whole viruses.[40] The identification of metabolites is complicated by the fact that blood contains thousands of chemically similar molecules. Hence, real-time analysis of the blood metabolome will require developing nanopores that contain a sensing element that recognizes and quantifies a molecule with high specificity.

We have recently shown that folded proteins pushed by the electroosmotic flow entered inside a cytolysin A (ClyA) nanopore. Notably, changes in the nanopore current could report the switching of the protein from its open unliganded conformation to its closed liganded conformation.[41] The frequency of switching from the open to the closed configurations is related to the concentration of the ligand in solution. The single-molecule nature of the nanopore approach allowed the simultaneous detection of multiple ligands.[42] This is because when a protein enters inside the nanopore, the associated blocked current can be used to identify the protein adaptor. Importantly, the concentration of the ligand could be measured directly from blood or other biological samples without any sample preparation,[42] indicating that this approach can be used in real-time blood analysis.

Some of the protein adaptors used in the initial experiments were substrate-binding proteins,[41,42] which are associated with bacterial ATP-binding cassette importers for substrate uptake.[43] Hundreds of such proteins exist that bind metabolites specifically,[44] which make them ideal in developing nanopore sensors for metabolites. However, several aspects of the nanoconfinement of the protein inside ClyA are unknown, including the origin of the signal for the open and closed states, the relation between the concentration of analytes in bulk and inside the nanopore, the positioning of proteins inside the nanopore, and the relation between the signal and the size and shape of the incorporated protein. Here, we study 13 possible adaptor proteins varying in size, shape, charge, and ligand. We found that the majority of proteins can be used to determine the concentration of their cognate ligands in bulk solution. The analysis of the protein blockades revealed that inside the ClyA nanopore proteins occupy two possible binding sites depending on the charge and size of the adaptor. Conveniently, the properties of the protein adaptors can be manipulated to improve the nanopore signal.

RESULTS AND DISCUSSION

Protein Adaptors. Thirteen different proteins were tested as adaptors in the ClyA-AS from *Salmonella typhi* nanopore (Figure 1). These proteins were recombinantly expressed in *E. coli* and purified (Figure S1) before being added to the nanopore. The protein sizes ranged from 25 to 42 kDa, and their net charge from 0 to −12, while their cognate ligands showed a variety of sizes, charges, and chemical properties (Table 1). In particular, the ligand charges ranged from +2 to −1; their size from 88 Da (putrescine, or 1,4-diaminobutane) to 1355 Da (CN-cobalamin, Figure 1b). Eleven of the 13 proteins were substrate-binding proteins of ABC transporters,
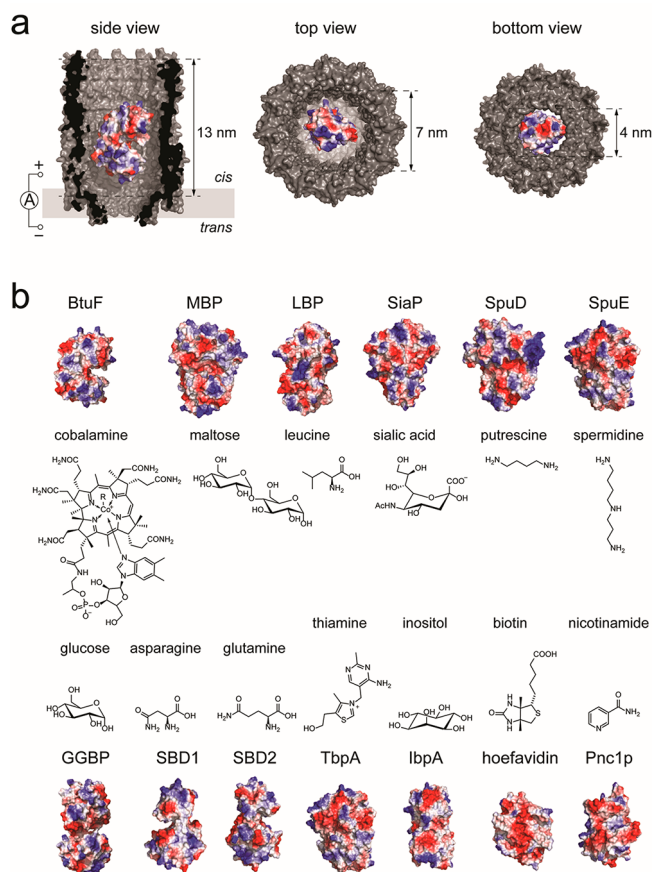

Figure 1. Protein adaptors for ClyA nanopores. (a) Cut-through of a surface representation of a ClyA nanopore (PDB: 2WCD) containing a single protein adaptor (BtuF, vitamin B12-binding protein, PDB: 1N2Z). (b) Surface representation of the 13 adaptor proteins studied in this work, and the chemical structure of their respective ligands. Proteins are colored according to their surface charge (Pymol). PDB files: MBP (maltose-binding protein): 1OMP; LBP (leucine-binding protein): 1USG; SiaP (sialic acid-binding protein): 4MMP; SpuD (putrescine-binding protein): 3TTM; SpuE (spermidine binding protein): 3TTL; GGBP (glucose-/galactose-binding protein): 2FVY; SBD1 (substrate-binding protein 1): 4KPT; SBD2 (substrate-binding protein 2): 4KR5; TbpA (thiamine-binding protein): 2QRY; IbpA (myo-inositol-binding protein): 4IRX; hoefavidin (dimeric avidin): 4Z27; Pnc1p (nicotinamidase): 3 V8E.

which are known to specifically bind metabolites through conformational changes involving large-scale domain motions.[45−47] In order to generalize our approach, as the shape- and the ligand-induced structural rearrangement of SBDs are comparable, we also tested two proteins from different families: nicotinamidase and hoefavidin. Nicotinamidase converts nicotinamide to nicotinic acid, which are part of the vitamin B3 system and are both metabolites and biomarkers.[48] Hoefavidin is a dimeric avidin that binds specifically biotin,[49] which is also known as vitamin B7.

Protein Signal. In a typical experiment, a negative potential is applied to the *trans* side of the nanopore, whereas proteins are added to the *cis* side (Figure 2a,b). The entry of the protein in the pore is observed by the specific reduction of the open pore current I_O to the blocked pore current I_B. In a 150 mM NaCl solution, pH 7.5, each protein adaptor showed an individual current signal as measured by the residual current

Table 1. Adaptor Proteins Used in This Work[a]

protein	PDB	ligand	protein size [kDa]	protein charge	ligand size [Da]	ligand charge	V [mV]	σ_B/σ_O	I_{RES} open [%]	I_{RES} closed [%]	K_D bulk [nM]	K_D pore [nM]
SBD1	4kpt	asparagine	25.5	−2	132.1	0	−70	1.45 ± 0.2	66.2 ± 0.4	65.4 ± 0.1	200[46]	470 ± 3[41]
Pnc1p	3v8e	nicotinamide	26.1	−9	122.1	0	−60	13.7 ± 2.2	55.8 ± 0.3	n.d.	n/a	n.d.
Pnc1p_dipole		nicotinamide	25.0	−6	122.1	0	−60	1.40 ± 0.2	n.d.	n.d.	n/a	n.d.
SBD2	4kr5	glutamine	27.8	−5	146.1	0	−70	0.87 ± 0.2	64.0 ± 0.3	62.9 ± 0.3	900[46]	830 ± 10[41]
BtuF	1n2z	CN-cobalamine	28.0	0	1355.4	0	−55	15.7 ± 8.5	68.0 ± 0.4	60.6 ± 0.5	14.8[50]	26 ± 8
hoefavidin	4z27	biotin	30.8	−12	244.3	0	−90	n.d.	n.d.	n.d.	358[49]	n.d.
IbpA	4irx	myo-inositol	31.8	−2	180.2	0	−60	7.52 ± 4.1	64.5 ± 0.5	n.d.	760[51]	n.d.
GGBP	2fvy	glucose	34.3	−6	180.2	0	−90	0.84 ± 0.0	68.3 ± 0.6	66.2 ± 0.7	200[52]	42 ± 3
SiaP	4mmp	sialic acid	35.2	−5	309.3	−1	−50	2.93 ± 0.9	58.1 ± 1.2	55.9 ± 1.4	19.7[53]	154 ± 18
TbpA	2qry	thiamine	36.5	−1	265.4	+1	−35	4.84 ± 3.4	49.8 ± 0.2	47.6 ± 0.1	33[54]	40 ± 10
LBP	1usg	leucine	38.0	−9	131.2	0	−60	3.24 ± 2.6	65.8 ± 0.3	60.2 ± 0.3	400[55]	86 ± 19
SpuE	3ttl	spermidine	38.8	−8	145.3	+2	−70	n.d.	n.d.	n.d.	14[56]	n.d.
SpuD	3ttm	putrescine	39.2	−3	88.2	+2	−80	0.74 ± 0.1	46.2 ± 0.7	44.0 ± 0.7	3[56]	2.3 ± 0.5
MBP	1omp	maltose	41.9	−9	342.3	0	−70	1.50 ± 0.3	59.3 ± 0.7	56.7 ± 0.8	1200[57]	1780 ± 240

[a]V represents the electric potential applied to the *trans* side of the nanopore. I_{RES} is the residual current after protein capture and was determined for the open and closed levels depicted in Figure 3. K_D is the apparent binding constant, and σ_B/σ_O is the signal-to-noise ratio of the protein adaptor. All experiments were performed in triplicates; the error represents the standard deviation.

$I_{RES} = 100 \times I_B/I_O$, the average residence time (τ), and the current noise (Figure 2). The latter is quantified using σ_B/σ_O, which is the standard deviation of the Gaussian distribution of the protein blockade (σ_B) divided by the standard deviation of the Gaussian distribution of the open pore (σ_O).

Three classes of signals were recorded (Figure 2c). GGBP, SBD1, SBD2, MBP, and SpuD (see the legend in Figure 1 for the full name of the proteins) showed a σ_B/σ_O of ∼1, or even <1 (Table 1), suggesting that such proteins are lodged in a well-defined minimum within the nanopore where Brownian motions are largely suppressed. Within this group, sometimes alternative blockades with higher noise levels occurred (*e.g.*, SpuD and MBP; see also Figures S2 and S7 for longer traces), which can be excluded from analysis. LBP, IbpA, TbpA, and SiaP showed a more dynamic but reproducible current signal with a σ_B/σ_O between 3 and 8, while Pnc1p and BtuF exhibited a σ_B/σ_O above 10. Multiple levels were observed within a blockade, suggesting that these proteins are either intrinsically dynamic or moving within the lumen of ClyA on a time scale similar to the sampling rate (20 μs). SpuE and hoefavidin represented a third kind of signal, in which each blockade showed a different signal (I_{RES} ranging from 44% to 57% for SpuE) and varying noise levels (Figure 2c). Since both proteins have a large net negative charge (net charge −12, hoefavidin) or are relatively large (39 kDa, net charge −8, SpuE), the unfavorable signal might originate from a combination of electrostatic and steric interactions with the nanopore inner surface.

In order to understand the origin of the highly dynamic protein blockades, we further investigated Pnc1p. Pnc1p has a net charge of −9 that is evenly spread across the surface of the protein, as shown by its net dipole perpendicular to the protein main axis (Figure 2d; see also Figure S15 for dipole of all tested proteins). If the dynamic current levels (σ_B/σ_O Pnc1p = 10) are reflecting the tumbling of the protein within the nanopore, then the introduction of a dipole on the protein surface should reduce the current noise. We introduced a negative charge at the C-terminus (K216E) and two positive charges (D82K, D83K) at the opposite end of the folded structure, and we deleted the C-terminal 6xHis-tag. The σ_B/σ_O decreased from 10 to 1 (Figure 2d), and the signal appeared

uniform and clear, suggesting correct folding. The noise reduction indicated that the highly dynamic signal was due to the fast tumbling of the protein inside the nanopore.

Current Modulation by Ligand Binding. In order to use adaptor proteins as sensors, the addition of ligands to the *cis* side of the nanopore should induce a change in the current signal. Nine of the tested proteins showed a change in the electrical signal when the ligands were added in the solution. For some proteins (SBD1, GGBP, SpuD, and TbpA, signal type 1a, Figures 3, S2, S3, S8, and S9), a single well-defined additional level corresponding to the shift from the open to the closed conformation of the protein was observed. Other proteins (LBP, SiaP, MBP, and BtuF, signal type 2, Figures 3 and S4−S7) showed often a noisy signal already in the unliganded form; thus the shift toward the closed conformation of the protein was more difficult to assign due to the high noise. Probably, intrinsic motions and unspecific interactions of the proteins with the nanopore are in this group more pronounced. SBD2 was a special case (classified type 1b), as the current blockade showed two well-defined current levels, and the addition of the ligand introduced a third well-defined level. Previous work demonstrated that the two levels of the *apo* protein correspond to the different orientation of the protein in the open configuration inside the nanopore, while the third level corresponds to the closed protein conformation.[41]

In all blockades the closed state showed less current compared to the open state. Since a more condensed structure is expected to block less current than a less condensed structure, this finding suggests that the signal is most likely associated with a change in the position of the protein within the pore. Most likely, as the structure of the protein becomes more compacted, the protein penetrates deeper inside the nanopore, resulting in more current being blocked (*i.e.*, less overall current). Interestingly, we also noticed that all the *apo* protein showed conformational transitions to the closed state also in the absence of their cognate ligand. This could reflect spontaneous opening and closing of the protein. Indeed, intrinsic conformational changes were observed for GGBP[58] and MBP[59] as well as SBD1 and SBD2,[46] in NMR and single-molecule fluorescence studies, respectively. However, this
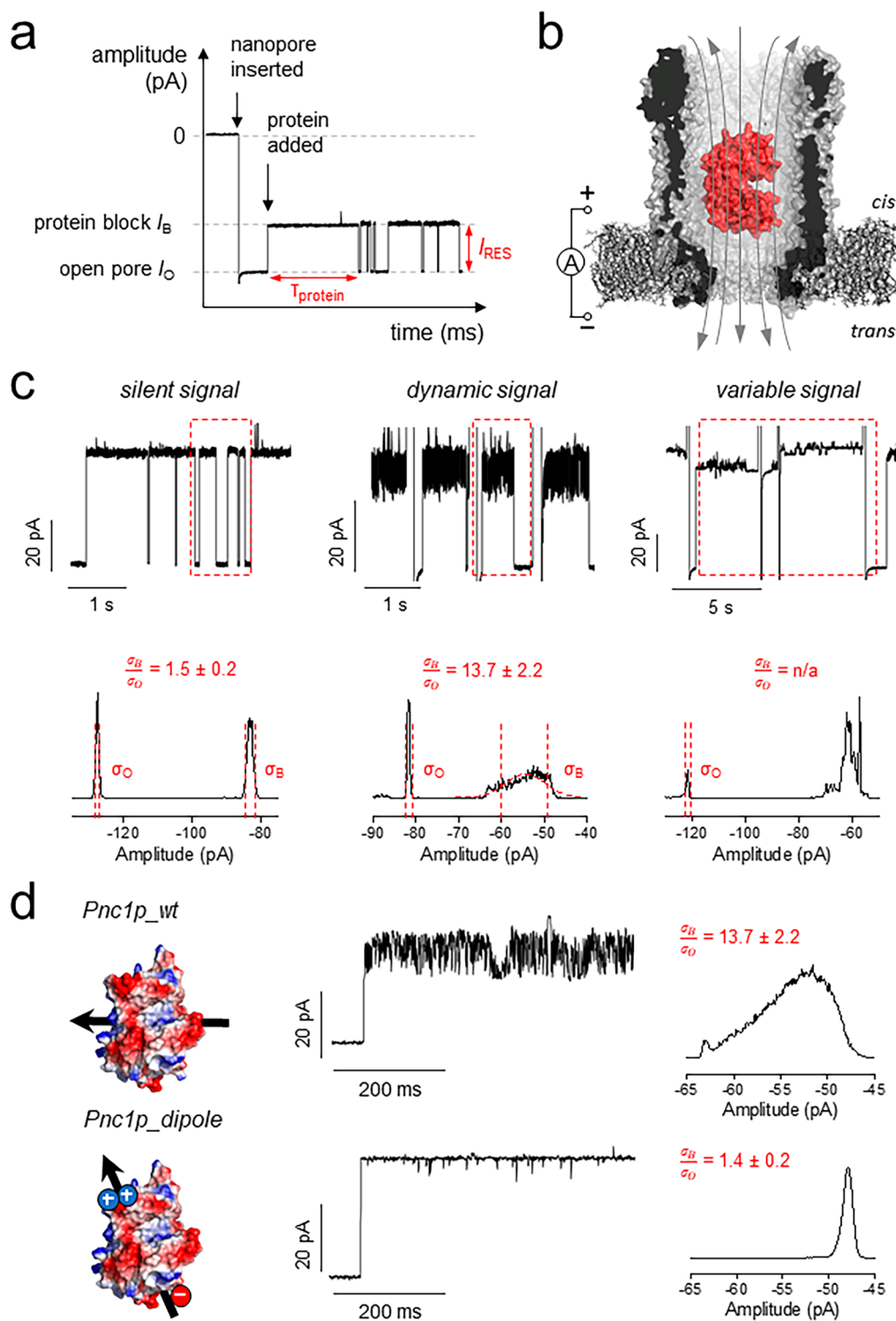
Figure 2. Protein signals in the ClyA-AS nanopore. (a) Typical trace showing the main measurands of an adaptor protein in the pore: dwell time ($\tau_{protein}$) and residual current ($I_{RES} = I_B/I_O \times 100\%$). In a typical experiment, thousands of dwell times are collected and exponential fits are used to determine the average $\tau_{protein}$. I_B and I_O were determined by Gaussian fitting to all-point histograms of protein blockades. (b) Representation of a protein (BtuF) electrophoretically captured in the pore. The gray arrows indicate the flux of ions across the nanopore. (c) Example of the three different signals and corresponding full-point histograms of a 1 s trace. σ_B/σ_O represents the ratio of the standard deviation of the Gaussian fitting of the open pore current and the protein block current as measured from full-point histograms. (d) Protein signal optimization. On the left: Surface representation of Pnc1p and Pnc1p_dipole (D82K, D83K, K216E, Δ6xHis) with the arrow showing the direction of the protein dipole. The current trace shows a typical protein blockade. The histograms were calculated from a representative 10 s of protein block. All measurements were performed in 15 mM Tris and 150 mM NaCl, pH 7.5, under negative bias (*trans*) and sampling at 10 kHz with a 2 kHz Bessel filter. For figure preparation, all traces were additionally filtered with a 500 Hz Gaussian filter.
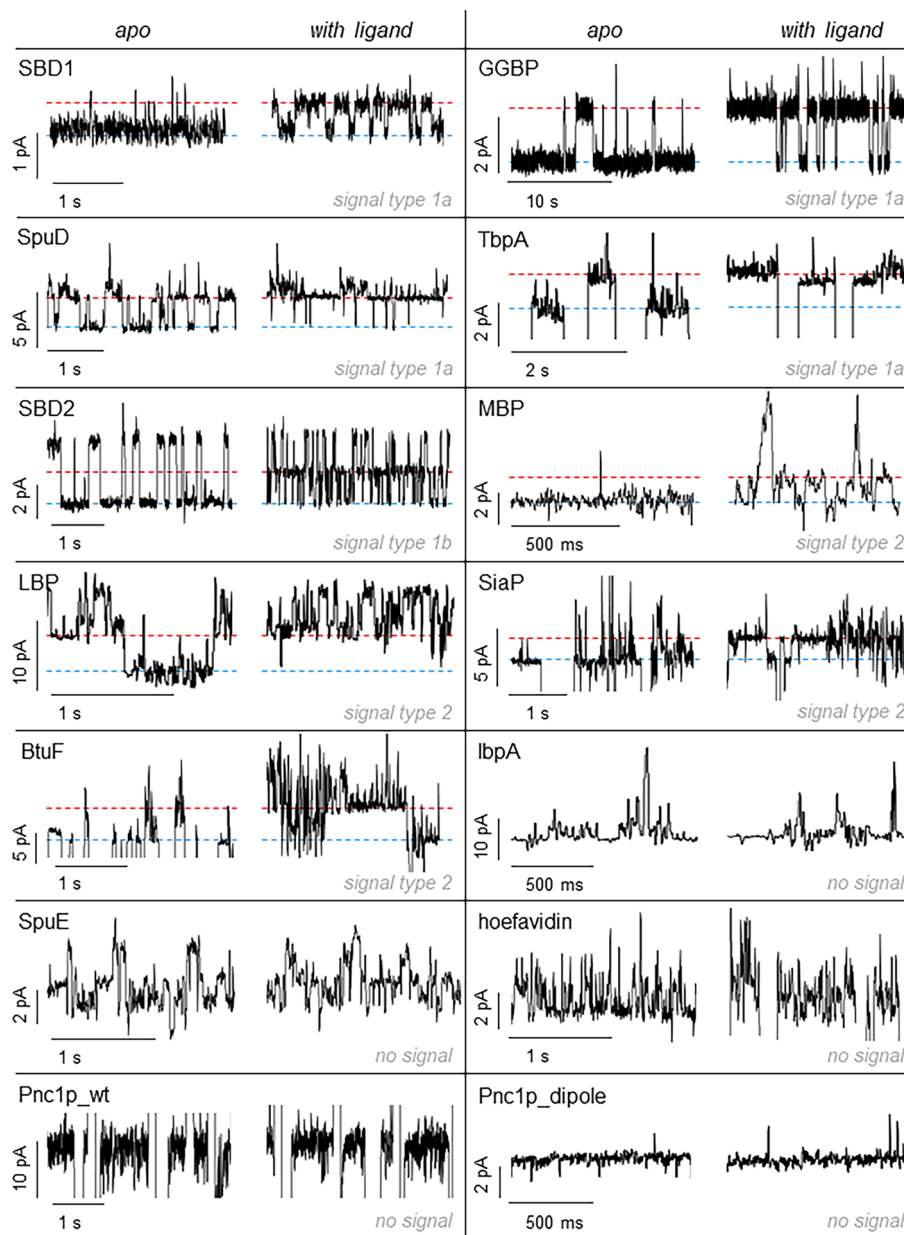
Figure 3. Current modulation of adaptor proteins upon ligand binding. In each box the left trace shows the current blockade of the *apo*-protein; the right the blockade in the presence of the cognate ligand added to the *cis* side. The ligand concentration for each protein was SBD1, 470 nM asparagine; GGBP, 500 nM glucose; SBD2, 2.4 μM glutamine; SpuD, 64 nM putrescine; BtuF, 500 nM CN-cobalamin; MBP, 2 μM maltose; LBP, 2 μM leucine; SiaP, 400 nM sialic acid; Tbpa, 2 μM thiamine; SpuE, 1 mM spermidine; IbpA, 40 μM myo-inositol; hoefavidin, 10 μM biotin; Pnc1p_wt, 2 mM nicotinamide; Pnc1p_dipole, 100 μM nicotinamide. The blue line represents the unbound state; the red line the bound state. All measurements were performed in 15 mM Tris and 150 mM NaCl, pH 7.5, under a negative bias (*trans*). Traces were sampled at 10 kHz and filtered with a 2 kHz Bessel filter. For figure preparation, all traces were additionally filtered with a 100 Hz Gaussian filter.

could also result from the binding of contaminant to the protein adaptors.

Hoefavidin, a dimeric avidin that binds to biotin, did not manifest ligand-induced signal changes. Previous work using a tetrameric avidin (60 kDa) revealed that the binding of biotin induced a conductance change in the *E. coli* ClyA nanopore.[60] Possibly, therefore, a tight fit between the protein and the pore is required to observe the rather small conformational change that follows the binding of biotin to avidin. Pnc1p and Pnc1p-dipole also showed no change in signal upon binding to nicotinamide, as well as two SBD proteins (Figure 3). These proteins have a comparable size and charge to other proteins

that display a ligand-induced signal (Table 1). Possibly, these proteins bind inside the nanopore in a configuration that prevents the ligands from reaching the active site or the conformational change upon ligand binding is too small to cause significant current alteration.

Affinity of Adaptor Proteins for Their Cognate Ligands. The ability of the nanopore sensor to identify analytes was tested by applying increasing concentration of ligands to the *cis* side of the nanopore and measuring the open and closed protein levels. In GGBP, SBD1, SBD2, and SpuD the association k_{on} and dissociation k_{off} rate constants could be measured by sampling the dwell time of the open (τ_{on}) and
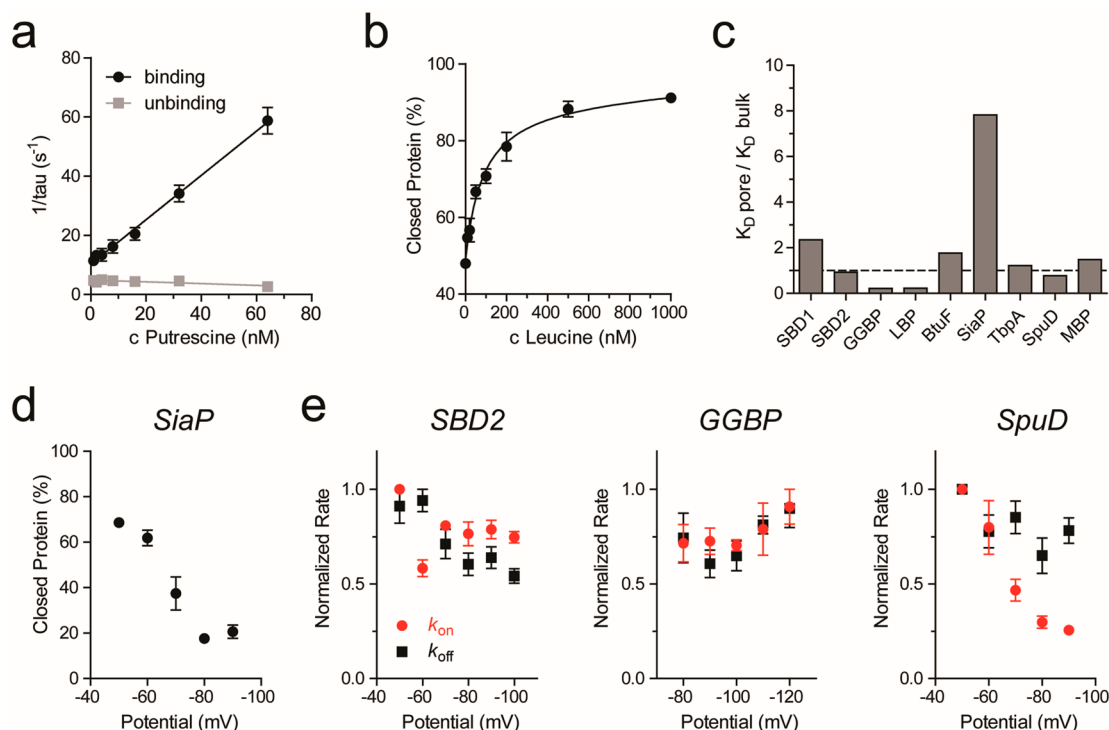
Figure 4. Dissociation constants and binding rates. (a) Representative example of rate constant determination. Binding and unbinding frequencies were determined from event dwell times (see also Figure S2bc). (b) Representative example of a ligand binding curve. The percentage of protein in the closed state was determined by the analysis of full-point histograms followed by ratio calculation of the peak height of the bound and unbound protein state over concentration (see also Figure S5bc). (c) Difference between the K_D determined in the nanopore (K_D pore) and the K_D reported in the literature (K_D bulk); see also Table 1. (d) Change in the percentage of SiaP in the closed state with increasing negative potential at a fixed sialic acid concentration of 150 nM. (e) Binding and unbinding rates for three different proteins with increasing negative potential at a fixed ligand concentration (SBD2: 830 nM glutamine; GGBP: 50 nM glucose; SpuD: 8 nM putrescine). K_{on} and k_{off} were determined and then normalized to the highest value of every measurement. All experiments were performed in triplicates. The error bars represent the standard error of the mean.

closed (τ_{off}) levels (Figure S2b,c). Typically, more than 500 events per condition were measured. k_{on} were then determined as $1/(\tau_{on}c_{ligand})$ and k_{off} as $1/\tau_{off}$. For this class of adaptors, the apparent binding constant K_D was measured by increasing the ligand concentration and observing the change in the binding frequency (Figure 4a). Conveniently, K_D can be also estimated at a single substrate concentration as k_{off}/k_{on}.

For the other proteins, because their binding rates could not be easily determined, the K_D was measured from full-point histograms of the whole trace (typically 2−3 min per concentration) based on the I_{RES} (see Experimental Section). Within the histogram, the peaks representing the open and ligand-bound (closed) protein were easily identified (Figure S2d,e). The K_D was then measured by plotting the fraction of the protein in the closed configuration (see Experimental Section) as a dependency of the ligand concentration and fitting on a binding curve (Figure 4b). BtuF displayed a noisy signal that prevented histogram analysis. However, K_D could still be determined by analyzing the fast-current blockades (see SI, Experimental Section, and Figure S6b,c).

The apparent K_D values measured by the nanopore were for six proteins comparable to the values measured in bulk (Table 1, Figure 4c). GGBP and LBP exhibited ~4-fold higher affinity then determined in bulk measurements. A notable exception was represented by the binding of sialic acid to SiaP, which showed an 8-fold higher K_D than in the bulk. A 100-fold decreased affinity compared to bulk values was also observed

for the binding of NADPH to DHFR[61,62] and for the binding of oxoglutarate to AlkB.[63] A possible explanation is that the diffusion of negatively charged ligands across the nanopore is retarded by the negative bias applied to the *trans* chamber. To test for this effect, we measured the voltage dependency of the k_{on} and k_{off} rates for SiaP (net charge of sialic acid −1), SBD2 and GGBP, which bind to glutamine and glucose, respectively (both neutral), and SpuD, which binds to putrescine (net charge +2) (Figure 4d,e). The signal of SiaP is complex and prevented measuring association and dissociation rate constants. Instead, we determined the fraction of the protein in the closed conformation as a function of the bias. We found that the fraction of SiaP in the closed state decreased with increasing potential (Figure 4d), which is compatible with an electrophoretic reduced diffusion of the negative ligand across the nanopore. According to this interpretation, when measuring neutral ligands (asparagine and glucose), the dissociation and association rate constants remained largely unaffected by the increased potential (Figure 4e). Unexpectedly, however, the binding frequency of positively charged spermidine to SpuD decreased four times by increasing the applied bias from −50 mV to −90 mV, while the dissociation rate remained constant. This is surprising, because the diffusion of putrescine toward the negative *trans* side is expected to be facilitated by the applied potential. A possible explanation is that SpuD, which is bigger than the other proteins tested (Table 1), sits tightly inside the nanopore. The
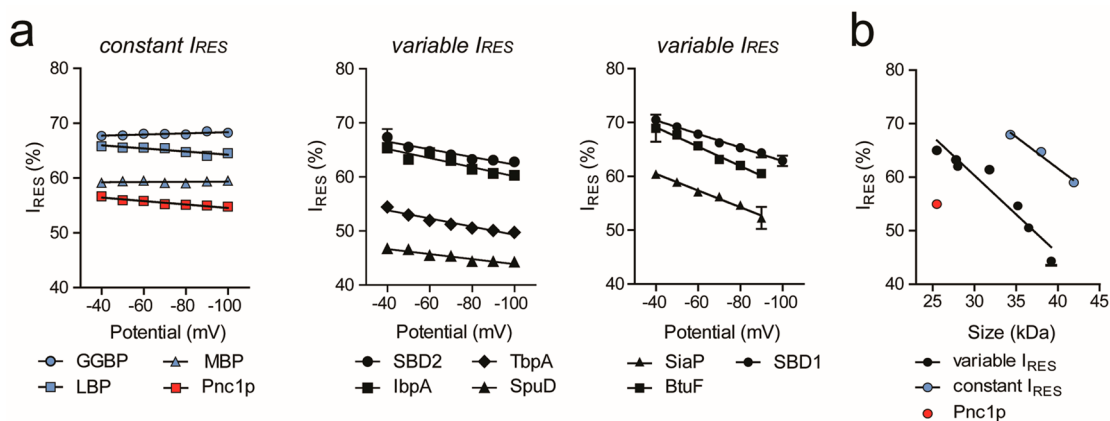
Figure 5. Characterization of the protein binding behavior in the nanopore. In the absence of ligands, a negative potential was applied to the *trans* side of the pore. All plots show the mean of at least three independent experiments. The threshold for classification as "constant I_{RES}" was set for linear fits with a slope ≤0.03. (a) Dependency of residual current (I_{RES}) on applied potential. I_{RES} is constant (blue, red) or variable (black) over potential. (b) I_{RES} obtained at −80 mV plotted against the protein size in kDa. The mutants TbpA Y27A, and Pnc1p_dipole were used.

increased electroosmotic flow may push the protein deeper inside the nanopore, thus reducing the accessibility of the ligand for its binding site. Noticeably, however, at −80 mV the K_D of SpuD is similar to the value measured in bulk (Figure 4c), suggesting that the effect of the potential does not significantly compromise the integrity of the protein inside the nanopore.

Two Protein Residence Sites inside the Nanopore. It is generally accepted that in nanopore experiments the current blockade arises from the excluded volume of the analyte inside the nanopore.[64,65] Hence, for a protein inside ClyA, the residual current is expected to depend on the size of the protein. However, the charge of the protein and its relative position within the nanopore are also likely to play a role. Two main forces drive proteins in and out the nanopore. Under a negative applied potential, the electrophoretic force moves negatively charged proteins toward the *cis* side, hence resisting their entry inside the pore. By contrast, the electroosmotic flow (EOF) moves the protein toward the *trans* side,[66,67] facilitating the entry of proteins inside the nanopore independently of the charge of the protein. The balance between these forces is, therefore, likely to define the I_{RES} and dwell time of proteins inside ClyA. We found that for all proteins the dwell time inside ClyA increased by about 10-fold every 10 mV (Figure S16), indicating that despite the charge of the protein, the EOF is the dominant force in driving the proteins inside the nanopore.[68,69] For five proteins (SBD1, SBD2, BtuF, IbpA, and GGBP) we observed a decrease in dwell time with the potential, suggesting that above a certain potential a protein can translocate through the nanopore.[62,70]

The voltage dependency of the proteins' I_{RES} showed two behaviors (Figure 5a). Noteworthy, SpuE and hoefavidin are not included in the analysis because of the too large variation in their signal. The I_{RES} of Pnc1p, GGBP, LBP, and MBP remained constant with the applied bias, while the I_{RES} of the other proteins decreased when increasing the potential. The former proteins have a relatively large negative net charge (−9, −9, −9, and −6, respectively, Table 1), suggesting that the *trans* to *cis* electrophoretic force almost perfectly opposes the *cis* to *trans* electroosmotic flow. By contrast, the reduced I_{RES} with the bias for the latter proteins most likely represent a deeper penetration of the protein toward the narrower *trans*

constriction of the nanopore as the EOF is increased. Interestingly, the blockades of the highly negatively charged proteins (LBP, MBP, and GGBP, but not Pnc1p) were associated with higher current compared to the blockade of the other group of proteins (Figure 5b). It has been previously shown that human thrombin (37 kDa, pI 8.8) occupies two residence sites (R1 and R2) within the lumen of the ClyA nanopore depending on the applied potential,[71] where R1 reflects a site located closer to the *cis* entrance of the nanopore and R2 a more sterically constrained site deeper in the pore.[72] Therefore, a possible explanation is that the large and/or highly negatively charged proteins occupy the more superficial R1 residence site, while smaller and less negatively charged proteins occupy the deeper R2 residence site.

CONCLUSIONS

The ability to sense metabolites in real-time using low-cost sensing devices is of great interest in personalized health-care monitoring.[5,6] We recently showed that nanopores with internalized protein adaptors can be used to quantify glucose and asparagine directly from biological samples.[42] Such adaptors belonged to the SBD protein family, which comprises more than 120 proteins that are capable of recognizing a variety of molecules including sugars, amino acids such as Glu, Ile, Val, Met, Pro, Arg, Cys, His, and GABA, metals such as tungsten, iron, and molybdenum, and vitamins such as riboflavin.[44,73] In this work we investigated 13 different protein adaptors, which bind to a wide range of metabolites (Figure 1). All proteins were tested under the same condition of pH (7.5) and ionic strength (150 mM NaCl), so that multiple protein adaptors could be used simultaneously under physiological conditions.

Ligand binding was detected in nine of the 11 SBD proteins examined within the ClyA nanopore, suggesting that the majority of SBDs are suitable adaptor proteins for metabolite sensing. Incidentally, the adaptors were either negatively charged or neutral, while their size comprised between 25 kDa (SBD1) and 42 kDa (MBP). Although a large negative charge reduced the residence time of the protein inside the nanopore, all proteins entered the nanopore and remained trapped for several seconds. The analysis of the current signal revealed that inside the nanopore proteins most likely occupy

two residence sites where they are in a relatively tight interaction with the nanopore lumen. Noisy signals were occasionally observed, and they most likely originated from the tumbling of the protein inside the nanopore with a frequency comparable to the sampling frequency (10 kHz) or the intrinsic motions of the protein itself. Nonetheless, the introduction of a dipole within the surface of the protein allowed orienting the protein with the electric field lines inside the nanopore and drastically reduced the current noise.

The affinity binding constant measured for the majority of the internalized proteins that bound to noncharged ligands compared reasonably well to bulk values, suggesting that the proteins remain folded inside the nanopore and that the concentration of ligands across the nanopore is comparable with bulk concentrations. It also suggests that the electrostatic interactions between the proteins and the interior of the nanopore, the relatively strong transmembrane electric fields, and the confinement of solvent inside the nanopore do not fundamentally change the function of proteins, which is rather surprising, as protein folding is known to be affected by electric fields in solid-state nanopores.[64,78] Nonetheless, the small deviation in affinity of the adaptors can be compensated for sensor application by the usage of standard curves. The association rates measured for charged ligands, however, depended on the applied potential, indicating that the diffusion of charged molecules is affected by the electric field drop inside the nanopore. This finding might be useful for a sensor as well, because the applied potential can be used to tune the affinity of the nanopore sensor for charged analytes.

Investigations with solid-state nanopores revealed that, despite the fact that the dipole and shape of the protein might be displayed by ionic currents,[74–77] the protein signal is originated almost exclusively by the excluded volume of the protein.[64,78,79] By contrast, by using biological nanopores such as ClyA, which has a size similar to the size of the protein adaptor, we found that the protein signal is also influenced by the position of the protein within the nanopore, which in turn is determined by a complex relation between the protein size, shape, surface charge distribution, and residence site occupancy. This is advantageous since the binding of ligands to the protein is likely to change the position of the protein within the nanopore, which in turn is reflected by a change in the signal that is used to detect the metabolite.

EXPERIMENTAL SECTION

Materials. All chemicals were purchased from Sigma-Aldrich, enzymes from Thermo Scientific, and DNA from Integrated DNA Technologies (IDT).

Cloning. The genes encoding for the proteins used in this work, which were designed to include NdeI and XhoI restriction sites, were first digested and then ligated to either pT7SC, pET22b, or pET101TOPO vectors. The resulting plasmids were transformed into E. coli cells to amplify the DNA. The identity of the plasmid was checked by sequencing. We used three different plasmids in this study, all controlled by a T7 promoter. pT7SC: ClyA, GGBP; pET101TOPO: TbpA, SiaP, LBP, SpuD, IbpA; pET22b: SpuE, BtuF, Pnc1p, hoefavidin, MBP. The point mutations D82K,D83K,K216E introduced into Pnc1p and the removal of the His-Tag on the C-terminus were done by a mega-primer PCR[80] followed by restriction with NdeI and XhoI and ligation to the pET22b vector.

Expression and Purification of ClyA Nanopores. ClyA nanopores were expressed and purified as previously reported.[42] In brief, the protein was expressed in E. coli BL21(DE3) cells in 2-YT medium. When the optical density at 600 nm reached 0.6, 0.5 mM

IPTG was added, the temperature was set to 25 °C, and the cells were grown for 20 h. Cells were then harvested by centrifugation (8000g, 5 min) and lysed by three freeze−thaw cycles and resuspension in lysis buffer containing 10 μg/mL lysozyme, 0.2 U/mL DNase, and 5 mM MgCl₂. After centrifugation at 7500 rpm for 30 min, the supernatant resulted from a 100 mL culture was loaded on 100 μL of Ni-NTA resin for purification utilizing the His-tag at the C-terminus of the protein. Proteins were eluted with 300 mM imidazole in Tris buffer (15 mM Tris, 150 mM NaCl, pH 7.5), and the protein was oligomerized with 0.2% β-dodecylmaltoside (DDM) for 30 min at 37 °C. Oligomers were separated from monomers using native polyacrylamide gel electrophoresis. The band corresponding to the 12-mer of ClyA was cut out, and the protein was extracted by adding 0.2% DDM and 10 mM EDTA in Tris buffer.

Expression and Purification of Adapter Proteins. Purified SBD1 and SBD2 were kindly provided by Bert Poolman, University of Groningen, and prepared as described before.[41] Purified MBP was kindly provided by Giorgos Gouridis, KU Leuven.

His₆MBP was expressed and purified as previously.[47] Briefly, cells harboring the plasmid expressing His₆MBP was introduced to E. coli BL21(DE3) cells and grown until an optical density (OD₆₀₀) of 0.5 was reached, and protein expression was induced by 0.25 mM isopropyl β-D-1-thiogalactopyranoside (IPTG). The soluble material (50 000 g, 30 min, 4 °C) was purified on a Ni²⁺-sepharose resin (equilibrated: 50 mM Tris-HCl, pH 8, 1 M KCl, 10% glycerol,10 mM imidazole; washed: 50 mM Tris-HCl, pH 8, 50 mM KCl, 10% glycerol, 10 mM imidazole and subsequently with 50 mM Tris-HCl, pH 8, 50 mM KCl, 10% glycerol, 30 mM imidazole; eluted: 50 mM Tris-HCl, pH 8, 50 mM KCl, 10% glycerol, 300 mM imidazole), concentrated (Amicon, Merck-Millipore), dialyzed (50 mM Tris-HCl, pH 8, 50 mM KCl, 50% glycerol), aliquoted, and stored at −20 °C.

For all other proteins, plasmids containing the desired gene were transformed in E. coli BL21(DE3), and a starter culture in 2-YT medium was grown at 37 °C overnight. The starter was transferred the next day in 100 mL of TB medium (or 2-YT medium for GGBP and TbpA) to an optical density of 0.15 and grown at 37 °C until OD ≥ 0.6. Expression was induced by addition of 0.5 mM IPTG, and cells were grown at 25 °C overnight. The next day, cells were harvested by centrifugation (8000g, 5 min). All periplasmic substrate binding proteins (BtuF, GGBP, IbpA, SiaP, TbpA, LBP) were prepared as follows: the pellet containing overexpressed proteins was resuspended in 50 mL of ice-cold sucrose buffer (20% sucrose, 50 mM Tris, 1 mM EDTA, pH 7.5) per 100 mL of culture and incubated with gentle shaking and cooling for 30 min. The suspension was centrifuged at 7500 rpm for 20 min, and the pellet was resuspended in 30 mL of ice-cold water, shaken, and centrifuged as before. The supernatant was taken for Ni-NTA purification. Hoefavidin and Pnc1p were prepared by resuspending the pellet containing overexpressed proteins in 10 mL of lysis buffer (1 mM MgCl₂, 0.2 U/mL Dnase I, 10 μg/mL lysozyme in protein buffer (150 mM NaCl, 15 mM Tris), pH 7.5), incubated 30 min at room temperature followed by 2 × 30 sweeps of sonication and 20 min of centrifugation at 7500 rpm.

All proteins except for hoefavidin were purified using Ni-NTA affinity chromatography. Typically the cell lysate containing the overexpressed protein was loaded on ca. 500 μL in protein buffer equilibrated Ni-NTA beads. The collected flow-through was loaded again to achieve maximum loading. The beads were washed with 20 mL of washing buffer (10 mM imidazole in protein buffer, pH 7.5). The protein was eluted with 5 mL of elution buffer (300 mM imidazole in protein buffer) in two steps and concentrated with Amicon centrifugal filters to a final volume of 500 μL. Hoefavidin was purified by affinity chromatography using 2-iminobiotin agarose beads (Sigma-Aldrich). The cell lysate was loaded twice on the beads using wash buffer (1 M NaCl, 50 mM Na₂CO₃, pH 11) followed by washing with 20 mL of the same wash buffer. Elution was obtained with 5 mL of elution buffer (50 mM NH₄CH₃CO₂, pH 4). The protein was concentrated with Amicon centrifugal filters. Buffer was changed to protein buffer (150 mM NaCl, 15 mM Tris, pH 7.5) by diluting 1:100 in protein buffer and concentrating again by using the Amicon filters. Protein concentrations were determined by absorption

measurement at 280 nm. Protein identity was confirmed by SDS-PAGE analysis. Proteins were stored with 20% glycerol at −80 °C.

Electrical Recordings in Planar Lipid Bilayers. The measuring setup consists of a vertical chamber containing two 500 μL compartments separated by a 20 μm PTFE film with a central aperture of ∼100 μm diameter. A lipid bilayer was formed on the aperture by adding a drop of hexadecane (2.5% (v/v) in pentane) on each side of the PTFE film directly above the aperture. After this, the compartments were filled with the recording buffer, and two drops of 1,2-diphytanoyl-*sn*-glycero-3-phosphocholine was added on each side. An electric potential was applied to the *trans* side utilizing Ag/AgCl electrodes. By lowering and raising the buffer level in one compartment across the aperture, a lipid bilayer was formed within the aperture. After letting the bilayer stabilize for 5 min, a pipet tip was dipped into the ClyA-AS solution and dipped afterward into the buffer of the *cis* compartment. The formation of single pores in the lipid bilayer was monitored by applying a −35 mV bias, resulting in a current of −60 pA. Adaptor proteins and ligands were added to the *cis* compartment. All experiments were done in triplicates, which means that three different single pores were used.

Electrophysiological Data Recording and Processing. Electrophysiological data were recorded under a negative potential, which was varied between −20 and −150 mV by using an Axopatch 200B patch clamp amplifier (Axon Instruments) connected to a DigiData 1440 A/D converter (Axon Instruments). The data were sampled with a frequency of 10 kHz, and a low-pass Bessel filter of 2 kHz was applied. After data recording, the traces were additionally filtered with a Gaussian low-pass filter with a 100 Hz cutoff. Data recording was executed using Clampex 10.7 software (Molecular Devices), and analysis was realized with Clampfit 10.7 software (Molecular Devices).

Analysis of Current Traces. Open pore (I_O) and protein block currents (I_B) were determined from Gaussian fits to all-point histograms using a bin width of 0.1 pA. I_{RES} are then calculated as $100 \times (I_B/I_O)$. Standard deviations of the mean values of Gaussian fits to all-point histograms of protein blockades (σ) were calculated from 1 s traces using Clampfit (Molecular Devices). The dwell times for proteins inside the nanopore were measured applying a single-channel search function in Clampfit (Molecular Devices). About 100 events at I_B were collected, binned, and fitted to a single exponential to determine the average dwell time (τ). Single-channel search and dwell time analysis were also used to determine the association and dissociation rate constants for the ligands to their cognate protein adaptor. For that, levels referring to the open and closed protein state were predefined and picked by the program. Events with a duration of less than 10 ms were ignored. We collected at least 500 events per level per concentration. Association and dissociation rates were then calculated as $1/\tau_{on}$ and $1/\tau_{off}$, respectively. $k_{on} = 1/(\tau_{on}c_{ligand})$ and $k_{off} = 1/\tau_{off}$. K_D were calculated for individual ligand concentrations and used to measure the K_D as k_{off}/k_{on}.

The K_D for BtuF was measured by performing single-channel searches (Clampfit, Molecular Devices) on individual current blockades. Once the open and closed protein levels were identified, an analysis was performed without excluding short events. We picked at least 1000 events. The relative time the protein spent on the closed configuration was then estimated by counting events on the closed and open levels. Although this analysis did not reveal the association and dissociation rate constant, we could plot the fraction of the overall number of events in the closed conformation *versus* the concentration of the ligand to produce binding curves that could be fitted to a binding isotherm (Prism5 software, GraphPad, one-site total fit) to determine K_D (Figure S6c).

K_D can also be determined by plotting all-point histograms of full traces (2−3 min length) based on the I_{RES} using a bin width of 0.1 pA. For that, I_O was determined as described above. All amplitude values within the histogram were divided by I_O to finally plot the I_{RES} *versus* the amount of data points. The resulting peaks corresponding to the open (no ligand bound) and the closed (ligand bound) protein conformation were then identified by changing the ligand concentration in the *cis* chamber. Typically one peak decreased

(protein's open form) and one peak increased (protein's closed form). We identified the I_{RES} of the peak maxima of the open and the closed state and determined the counts at this particular I_{RES} for the open state (N_O) and the closed state (N_C) at different ligand concentrations (added to the *cis* chamber). Parts of the histogram that did not change with the concentration of the ligands were excluded from histogram analysis (*e.g.*, for SpuD, Figure S2). The amount of closed protein in the sample was calculated by $N_C/(N_C + N_O)$ and was plotted against ligand concentration to fit a binding isotherm and to calculate the respective K_D. Full-point histograms corresponding to GGBP, SBD1, and SBD2 blockades showed well-defined peaks corresponding to the open and closed states. Hence, for these proteins a Gaussian fit was performed, and the area under the curve was used to calculate the fraction of the protein in the closed conformation.

ASSOCIATED CONTENT

ⓈI Supporting Information

The Supporting Information is available free of charge at https://pubs.acs.org/doi/10.1021/acsnano.9b09434.

Figures S1−S16: SDS-PAGE of purified adaptor proteins, exemplary traces for all tested proteins including description of dissociation constant determination, dipole orientation of all tested proteins, voltage dependency of the protein dwell time. (PDF)

AUTHOR INFORMATION

Corresponding Author

Giovanni Maglia − *Groningen Biomolecular Sciences & Biotechnology Institute, University of Groningen, 9747 AG Groningen, The Netherlands;* ⓞ orcid.org/0000-0003-2784-0811; Email: g.maglia@rug.nl

Authors

Sarah Zernia − *Groningen Biomolecular Sciences & Biotechnology Institute, University of Groningen, 9747 AG Groningen, The Netherlands;* ⓞ orcid.org/0000-0002-7513-5765

Nieck Jordy van der Heide − *Groningen Biomolecular Sciences & Biotechnology Institute, University of Groningen, 9747 AG Groningen, The Netherlands*

Nicole Stéphanie Galenkamp − *Groningen Biomolecular Sciences & Biotechnology Institute, University of Groningen, 9747 AG Groningen, The Netherlands*

Giorgos Gouridis − *Rega Institute for Medical Research, Laboratory of Molecular Bacteriology, KU Leuven, 3000 Leuven, Belgium*

Complete contact information is available at:
https://pubs.acs.org/10.1021/acsnano.9b09434

Author Contributions

S.Z. and G.M. designed the study and wrote the paper. S.Z. performed all experiments unless otherwise stated, analyzed data, and wrote the paper. N.H. cloned TbpA, SiaP, LBP, SpuD, and IbpA and expressed and purified TbpA. In addition, NH expressed, purified, and oligomerized the ClyA-AS nanopore. N.G. cloned, expressed, and purified GGBP and performed electrophysiological measurements of GGBP. G.G. cloned, expressed, and purified MBP. G.M. supervised the project. All authors verified the manuscript.

Notes

The authors declare no competing financial interest.

ACKNOWLEDGMENTS

REFERENCES

(1) Wishart, D. S.; Tzur, D.; Knox, C.; Eisner, R.; Guo, A. C.; Young, N.; Cheng, D.; Jewell, K.; Arndt, D.; Sawhney, S.; Fung, C.; Nikolai, L.; Lewis, M.; Coutouly, M.-A.; Forsythe, I.; Tang, P.; Shrivastava, S.; Jeroncic, K.; Stothard, P.; Amegbey, G.; et al. HMDB: The Human Metabolome Database. *Nucleic Acids Res.* **2007**, *35*, D521−526.

(2) Dunn, W. B.; Broadhurst, D.; Begley, P.; Zelena, E.; Francis-McIntyre, S.; Anderson, N.; Brown, M.; Knowles, J. D.; Halsall, A.; Haselden, J. N.; Nicholls, A. W.; Wilson, I. D.; Kell, D. B.; Goodacre, R. Procedures for Large-Scale Metabolic Profiling of Serum and Plasma Using Gas Chromatography and Liquid Chromatography Coupled to Mass Spectrometry. *Nat. Protoc.* **2011**, *6*, 1060−1083.

(3) Fiehn, O.; Kind, T. Metabolite Profiling in Blood Plasma. In *Metabolomics*; Weckwerth, W., Ed.; Walker, J. M., Series Ed.; Humana Press: Totowa, NJ, 2007; Vol. *358*, pp 3−17.

(4) Raamsdonk, L. M.; Teusink, B.; Broadhurst, D.; Zhang, N.; Hayes, A.; Walsh, M. C.; Berden, J. A.; Brindle, K. M.; Kell, D. B.; Rowland, J. J.; Westerhoff, H. V.; van Dam, K.; Oliver, S. G. A Functional Genomics Strategy That Uses Metabolome Data to Reveal the Phenotype of Silent Mutations. *Nat. Biotechnol.* **2001**, *19*, 45−50.

(5) Nicholson, J. K.; Holmes, E.; Wilson, I. D. Gut Microorganisms, Mammalian Metabolism and Personalized Health Care. *Nat. Rev. Microbiol.* **2005**, *3*, 431−438.

(6) Beger, R. D. A Review of Applications of Metabolomics in Cancer. *Metabolites* **2013**, *3*, 552−574.

(7) Nicholson, J. K.; Everett, J. R.; Lindon, J. C. Longitudinal Pharmacometabonomics for Predicting Patient Responses to Therapy: Drug Metabolism, Toxicity and Efficacy. *Expert Opin. Drug Metab. Toxicol.* **2012**, *8*, 135−139.

(8) van der Greef, J.; Hankemeier, T.; McBurney, R. N. Metabolomics-Based Systems Biology and Personalized Medicine: Moving towards n = 1 Clinical Trials? *Pharmacogenomics* **2006**, *7*, 1087−1094.

(9) Zhang, A.; Sun, H.; Wang, X. Serum Metabolomics as a Novel Diagnostic Approach for Disease: A Systematic Review. *Anal. Bioanal. Chem.* **2012**, *404*, 1239−1245.

(10) Kaddurah-Daouk, R.; Kristal, B. S.; Weinshilboum, R. M. Metabolomics: A Global Biochemical Approach to Drug Response and Disease. *Annu. Rev. Pharmacol. Toxicol.* **2008**, *48*, 653−683.

(11) Jiang, Y.; Zhu, Z.; Shi, J.; An, Y.; Zhang, K.; Wang, Y.; Li, S.; Jin, L.; Ye, W.; Cui, M.; Chen, X. Metabolomics in the Development and Progression of Dementia: A Systematic Review. *Front. Neurosci.* **2019**, *13*, 343.

(12) Yap, I. K. S.; Brown, I. J.; Chan, Q.; Wijeyesekera, A.; Garcia-Perez, I.; Bictash, M.; Loo, R. L.; Chadeau-Hyam, M.; Ebbels, T.; De Iorio, M.; Maibaum, E.; Zhao, L.; Kesteloot, H.; Daviglus, M. L.; Stamler, J.; Nicholson, J. K.; Elliott, P.; Holmes, E. Metabolome-Wide Association Study Identifies Multiple Biomarkers That Discriminate North and South Chinese Populations at Differing Risks of Cardiovascular Disease: Intermap Study. *J. Proteome Res.* **2010**, *9*, 6647−6654.

(13) Wang, T. J.; Larson, M. G.; Vasan, R. S.; Cheng, S.; Rhee, E. P.; McCabe, E.; Lewis, G. D.; Fox, C. S.; Jacques, P. F.; Fernandez, C.; O'Donnel, C. J.; Carr, S. A.; Mootha, V. K.; Flores, J. C.; Souza, A.; Melander, O.; Clish, C. B.; Gerszten, R. E. Metabolite Profiles and the Risk of Developing Diabetes. *Nat. Med.* **2011**, *17*, 448−453.

(14) Liesenfeld, D. B.; Habermann, N.; Owen, R. W.; Scalbert, A.; Ulrich, C. M. Review of Mass Spectrometry−Based Metabolomics in Cancer Research. *Cancer Epidemiol., Biomarkers Prev.* **2013**, *22*, 2182−2201.

(15) Sillanaukee; Pönniö; Jääskeläinen. Occurrence of Sialic Acids in Healthy Humans and Different Disorders. *Eur. J. Clin. Invest.* **1999**, *29*, 413−425.

(16) Fuhrer, T.; Zamboni, N. High-Throughput Discovery Metabolomics. *Curr. Opin. Biotechnol.* **2015**, *31*, 73−78.

(17) Manzi, M.; Riquelme, G.; Zabalegui, N.; Monge, M. E. Improving Diagnosis of Genitourinary Cancers: Biomarker Discovery Strategies through Mass Spectrometry-Based Metabolomics. *J. Pharm. Biomed. Anal.* **2020**, *178*, 112905.

(18) Kasianowicz, J. J.; Brandin, E.; Branton, D.; Deamer, D. W. Characterization of Individual Polynucleotide Molecules Using a Membrane Channel. *Proc. Natl. Acad. Sci. U. S. A.* **1996**, *93*, 13770−13773.

(19) Butler, T. Z.; Pavlenok, M.; Derrington, I. M.; Niederweis, M.; Gundlach, J. H. Single-Molecule DNA Detection with an Engineered MspA Protein Nanopore. *Proc. Natl. Acad. Sci. U. S. A.* **2008**, *105*, 20647−20652.

(20) Nomidis, S. K.; Hooyberghs, J.; Maglia, G.; Carlon, E. DNA Capture into the ClyA Nanopore: Diffusion-Limited *versus* Reaction-Limited Processes. *J. Phys.: Condens. Matter* **2018**, *30*, 304001.

(21) Moon, J.; Kim, N.; Kim, T.-J.; Jun, J.-S.; Lee, H. S.; Shin, H.-R.; Lee, S.-T.; Jung, K.-H.; Park, K.-I.; Jung, K.-Y.; Kim, M.; Lee, S. K.; Chu, K. Rapid Diagnosis of Bacterial Meningitis by Nanopore 16S Amplicon Sequencing: A Pilot Study. *Int. J. Med. Microbiol.* **2019**, *309*, 151338.

(22) Branton, D.; Deamer, D. W.; Marziali, A.; Bayley, H.; Benner, S. A.; Butler, T.; Di Ventra, M.; Garaj, S.; Hibbs, A.; Huang, X.; Jovanovich, S. B.; Krstic, P. S.; Lindsay, S.; Ling, X. S.; Mastrangelo, C. H.; Meller, A.; Oliver, J. S.; Pershin, Y. V.; Ramsey, J. M.; Riehn, R.; et al. The Potential and Challenges of Nanopore Sequencing. *Nat. Biotechnol.* **2008**, *26*, 1146−1153.

(23) Huang, G.; Willems, K.; Soskine, M.; Wloka, C.; Maglia, G. Electro-Osmotic Capture and Ionic Discrimination of Peptide and Protein Biomarkers with FraC Nanopores. *Nat. Commun.* **2017**, *8*, 935.

(24) Huang, G.; Voet, A.; Maglia, G. FraC Nanopores with Adjustable Diameter Identify the Mass of Opposite-Charge Peptides with 44 Da Resolution. *Nat. Commun.* **2019**, *10*, 835.

(25) Li, X.; Huang, J.; Holden, M. A.; Chen, M. Peptide-Mediated Membrane Transport of Macromolecular Cargo Driven by Membrane Asymmetry. *Anal. Chem.* **2017**, *89*, 12369−12374.

(26) Larimi, M. G.; Mayse, L. A.; Movileanu, L. Interactions of a Polypeptide with a Protein Nanopore Under Crowding Conditions. *ACS Nano* **2019**, *13*, 4469−4477.

(27) Fahie, M. A.; Yang, B.; Pham, B.; Chen, M. Tuning the Selectivity and Sensitivity of an OmpG Nanopore Sensor by Adjusting Ligand Tether Length. *ACS Sens.* **2016**, *1*, 614−622.

(28) Pastoriza-Gallego, M.; Rabah, L.; Gibrat, G.; Thiebot, B.; van der Goot, F. G.; Auvray, L.; Betton, J.-M.; Pelta, J. Dynamics of Unfolded Protein Transport through an Aerolysin Pore. *J. Am. Chem. Soc.* **2011**, *133*, 2923−2931.

(29) Thakur, A. K.; Movileanu, L. Real-Time Measurement of Protein−Protein Interactions at Single-Molecule Resolution Using a Biological Nanopore. *Nat. Biotechnol.* **2019**, *37*, 96−101.

(30) Bell, N. A. W.; Keyser, U. F. Specific Protein Detection Using Designed DNA Carriers and Nanopores. *J. Am. Chem. Soc.* **2015**, *137*, 2035−2041.

(31) Bell, N. A. W.; Keyser, U. F. Digitally Encoded DNA Nanostructures for Multiplexed, Single-Molecule Protein Sensing with Nanopores. *Nat. Nanotechnol.* **2016**, *11*, 645−651.

(32) Si, W.; Aksimentiev, A. Nanopore Sensing of Protein Folding. *ACS Nano* **2017**, *11*, 7091−7100.

(33) Li, X.; Lee, K.; Chen, J.; Chen, M. A ClyA Nanopore Tweezer for Analysis of Functional States of Protein-Ligand Interactions. *bioRxiv* **2019**, 727503 (accessed Jan 31, 2020).

(34) Ohayon, S.; Girsault, A.; Nasser, M.; Shen-Orr, S.; Meller, A. Simulation of Single-Protein Nanopore Sensing Shows Feasibility for Whole-Proteome Identification. *PLoS Comput. Biol.* **2019**, *15*, No. e1007067.

(35) Varongchayakul, N.; Song, J.; Meller, A.; Grinstaff, M. W. Single-Molecule Protein Sensing in a Nanopore: A Tutorial. *Chem. Soc. Rev.* **2018**, *47*, 8512−8524.

(36) Guo, Y.; Niu, A.; Jian, F.; Wang, Y.; Yao, F.; Wei, Y.; Tian, L.; Kang, X. Metal−Organic Complex-Functionalized Protein Nanopore Sensor for Aromatic Amino Acids Chiral Recognition. *Analyst* **2017**, *142*, 1048−1053.

(37) Boersma, A. J.; Bayley, H. Continuous Stochastic Detection of Amino Acid Enantiomers with a Protein Nanopore. *Angew. Chem., Int. Ed.* **2012**, *51*, 9606−9609.

(38) Boersma, A. J.; Brain, K. L.; Bayley, H. Real-Time Stochastic Detection of Multiple Neurotransmitters with a Protein Nanopore. *ACS Nano* **2012**, *6*, 5304−5308.

(39) Ramsay, W. J.; Bayley, H. Single-Molecule Determination of the Isomers of d-Glucose and d-Fructose That Bind to Boronic Acids. *Angew. Chem., Int. Ed.* **2018**, *57*, 2841−2845.

(40) Miyagawa, T.; Hongo, S.; Nakamura, N.; Horiguchi, Y.; Miyahara, Y.; Shibata, H. A Novel Diagnostic System for Infectious Diseases Using Solid-State Nanopore Devices. In *2018 40th Annual International Conference of the IEEE Engineering in Medicine and Biology Society (EMBC)*; 2018; pp 2833−2836.

(41) Van Meervelt, V.; Soskine, M.; Singh, S.; Schuurman-Wolters, G. K.; Wijma, H. J.; Poolman, B.; Maglia, G. Real-Time Conformational Changes and Controlled Orientation of Native Proteins Inside a Protein Nanoreactor. *J. Am. Chem. Soc.* **2017**, *139*, 18640−18646.

(42) Galenkamp, N. S.; Soskine, M.; Hermans, J.; Wloka, C.; Maglia, G. Direct Electrical Quantification of Glucose and Asparagine from Bodily Fluids Using Nanopores. *Nat. Commun.* **2018**, *9*, 4085.

(43) Tanaka, K. J.; Song, S.; Mason, K.; Pinkett, H. W. Selective Substrate Uptake: The Role of ATP-Binding Cassette (ABC) Importers in Pathogenesis. *Biochim. Biophys. Acta, Biomembr.* **2018**, *1860*, 868−877.

(44) Berntsson, R. P.-A.; Smits, S. H. J.; Schmitt, L.; Slotboom, D.-J.; Poolman, B. A Structural Classification of Substrate-Binding Proteins. *FEBS Lett.* **2010**, *584*, 2606−2617.

(45) Husada, F.; Gouridis, G.; Vietrov, R.; Schuurman-Wolters, G. K.; Ploetz, E.; de Boer, M.; Poolman, B.; Cordes, T. Watching Conformational Dynamics of ABC Transporters with Single-Molecule Tools. *Biochem. Soc. Trans.* **2015**, *43*, 1041−1047.

(46) Gouridis, G.; Schuurman-Wolters, G. K.; Ploetz, E.; Husada, F.; Vietrov, R.; de Boer, M.; Cordes, T.; Poolman, B. Conformational Dynamics in Substrate-Binding Domains Influences Transport in the ABC Importer GlnPQ. *Nat. Struct. Mol. Biol.* **2015**, *22*, 57−64.

(47) de Boer, M.; Gouridis, G.; Vietrov, R.; Begg, S. L.; Schuurman-Wolters, G. K.; Husada, F.; Eleftheriadis, N.; Poolman, B.; McDevitt, C. A.; Cordes, T. Conformational and Dynamic Plasticity in Substrate-Binding Proteins Underlies Selective Transport in ABC Importers. *eLife* **2019**, *8*, No. e44652.

(48) Seiner, D. R.; Hegde, S. S.; Blanchard, J. S. Kinetics and Inhibition of Nicotinamidase from Mycobacterium Tuberculosis. *Biochemistry* **2010**, *49*, 9613−9619.

(49) Avraham, O.; Meir, A.; Fish, A.; Bayer, E. A.; Livnah, O. Hoefavidin: A Dimeric Bacterial Avidin with a C-Terminal Binding Tail. *J. Struct. Biol.* **2015**, *191*, 139−148.

(50) Cadieux, N.; Bradbeer, C.; Reeger-Schneider, E.; Koster, W.; Mohanty, A. K.; Wiener, M. C.; Kadner, R. J. Identification of the Periplasmic Cobalamin-Binding Protein BtuF of Escherichia Coli. *J. Bacteriol.* **2002**, *184*, 706−717.

(51) Herrou, J.; Crosson, S. Myo-Inositol and d-Ribose Ligand Discrimination in an ABC Periplasmic Binding Protein. *J. Bacteriol.* **2013**, *195*, 2379−2388.

(52) Miller, D. M.; Olson, J. S.; Pflugrath, J. W.; Quiocho, F. A. Rates of Ligand Binding to Periplasmic Proteins Involved in Bacterial Transport and Chemotaxis. *J. Biol. Chem.* **1983**, *258*, 13665−13672.

(53) Gangi Setty, T.; Cho, C.; Govindappa, S.; Apicella, M. A.; Ramaswamy, S. Bacterial Periplasmic Sialic Acid-Binding Proteins Exhibit a Conserved Binding Site. *Acta Crystallogr., Sect. D: Biol. Crystallogr.* **2014**, *70*, 1801−1811.

(54) Hanes, J. W.; Chatterjee, D.; Soriano, E. V.; Ealick, S. E.; Begley, T. P. Construction of a Thiamin Sensor from the Periplasmic Thiamin Binding Protein. *Chem. Commun.* **2011**, *47*, 2273−2275.

(55) Magnusson, U.; Salopek-Sondi, B.; Luck, L. A.; Mowbray, S. L. X-Ray Structures of the Leucine-Binding Protein Illustrate Conformational Changes and the Basis of Ligand Specificity. *J. Biol. Chem.* **2004**, *279*, 8747−8752.

(56) Wu, D.; Lim, S. C.; Dong, Y.; Wu, J.; Tao, F.; Zhou, L.; Zhang, L.-H.; Song, H. Structural Basis of Substrate Binding Specificity Revealed by the Crystal Structures of Polyamine Receptors SpuD and SpuE from Pseudomonas Aeruginosa. *J. Mol. Biol.* **2012**, *416*, 697−712.

(57) Telmer, P. G.; Shilton, B. H. Insights into the Conformational Equilibria of Maltose-Binding Protein by Analysis of High Affinity Mutants. *J. Biol. Chem.* **2003**, *278*, 34555−34567.

(58) Unione, L.; Ortega, G.; Mallagaray, A.; Corzana, F.; Pérez-Castells, J.; Canales, A.; Jiménez-Barbero, J.; Millet, O. Unraveling the Conformational Landscape of Ligand Binding to Glucose/Galactose-Binding Protein by Paramagnetic NMR and MD Simulations. *ACS Chem. Biol.* **2016**, *11*, 2149−2157.

(59) Millet, O.; Hudson, R. P.; Kay, L. E. The Energetic Cost of Domain Reorientation in Maltose-Binding Protein as Studied by NMR and Fluorescence Spectroscopy. *Proc. Natl. Acad. Sci. U. S. A.* **2003**, *100*, 12700−12705.

(60) Lu, B.; Stokes, C.; Fahie, M.; Chen, M.; Golovchenko, J. A.; Hau, L. V. Protein Motion and Configurations in a Form-Fitting Nanopore: Avidin in ClyA. *Biophys. J.* **2018**, *115*, 801−808.

(61) Penner, M. H.; Frieden, C. Kinetic Analysis of the Mechanism of Escherichia Coli Dihydrofolate Reductase. *J. Biol. Chem.* **1987**, *262*, 15908−15914.

(62) Willems, K.; Ruić, D.; Biesemans, A.; Galenkamp, N. S.; Van Dorpe, P.; Maglia, G. Engineering and Modeling the Electrophoretic Trapping of a Single Protein Inside a Nanopore. *ACS Nano* **2019**, *13*, 9980−9992.

(63) Soskine, M.; Biesemans, A.; Maglia, G. Single-Molecule Analyte Recognition with ClyA Nanopores Equipped with Internal Protein Adaptors. *J. Am. Chem. Soc.* **2015**, *137*, 5793−5797.

(64) Talaga, D. S.; Li, J. Single-Molecule Protein Unfolding in Solid State Nanopores. *J. Am. Chem. Soc.* **2009**, *131*, 9287−9297.

(65) Li, J.; Fologea, D.; Rollings, R.; Ledden, B. Characterization of Protein Unfolding with Solid-State Nanopores. *Protein Pept. Lett.* **2014**, *21*, 256−265.

(66) Schoch, R. B.; Han, J.; Renaud, P. Transport Phenomena in Nanofluidics. *Rev. Mod. Phys.* **2008**, *80*, 839−883.

(67) Bhamidimarri, S. P.; Prajapati, J. D.; van den Berg, B.; Winterhalter, M.; Kleinekathöfer, U. Role of Electroosmosis in the Permeation of Neutral Molecules: CymA and Cyclodextrin as an Example. *Biophys. J.* **2016**, *110*, 600−611.

(68) Firnkes, M.; Pedone, D.; Knezevic, J.; Döblinger, M.; Rant, U. Electrically Facilitated Translocations of Proteins through Silicon Nitride Nanopores: Conjoint and Competitive Action of Diffusion, Electrophoresis, and Electroosmosis. *Nano Lett.* **2010**, *10*, 2162−2167.

(69) Gu, L.-Q.; Cheley, S.; Bayley, H. Electroosmotic Enhancement of the Binding of a Neutral Molecule to a Transmembrane Pore. *Proc. Natl. Acad. Sci. U. S. A.* **2003**, *100*, 15498−15503.

(70) Biesemans, A.; Soskine, M.; Maglia, G. A Protein Rotaxane Controls the Translocation of Proteins across a ClyA Nanopore. *Nano Lett.* **2015**, *15*, 6076−6081.

(71) Soskine, M.; Biesemans, A.; Moeyaert, B.; Cheley, S.; Bayley, H.; Maglia, G. An Engineered ClyA Nanopore Detects Folded Target Proteins by Selective External Association and Pore Entry. *Nano Lett.* **2012**, *12*, 4895−4900.

(72) Soskine, M.; Biesemans, A.; De Maeyer, M.; Maglia, G. Tuning the Size and Properties of ClyA Nanopores Assisted by Directed Evolution. *J. Am. Chem. Soc.* **2013**, *135*, 13456−13463.

(73) Scheepers, G. H.; Lycklama A Nijeholt, J. A.; Poolman, B. An Updated Structural Classification of Substrate-Binding Proteins. *FEBS Lett.* **2016**, *590*, 4393−4401.

(74) Houghtaling, J.; Ying, C.; Eggenberger, O. M.; Fennouri, A.; Nandivada, S.; Acharjee, M.; Li, J.; Hall, A. R.; Mayer, M. Estimation of Shape, Volume, and Dipole Moment of Individual Proteins Freely Transiting a Synthetic Nanopore. *ACS Nano* **2019**, *13*, 5231−5242.

(75) Yusko, E. C.; Bruhn, B. R.; Eggenberger, O. M.; Houghtaling, J.; Rollings, R. C.; Walsh, N. C.; Nandivada, S.; Pindrus, M.; Hall, A. R.; Sept, D.; Li, J.; Kalonia, D. S.; Mayer, M. Real-Time Shape Approximation and Fingerprinting of Single Proteins Using a Nanopore. *Nat. Nanotechnol.* **2017**, *12*, 360−367.

(76) Waduge, P.; Hu, R.; Bandarkar, P.; Yamazaki, H.; Cressiot, B.; Zhao, Q.; Whitford, P. C.; Wanunu, M. Nanopore-Based Measurements of Protein Size, Fluctuations, and Conformational Changes. *ACS Nano* **2017**, *11*, 5706−5716.

(77) Hu, R.; Rodrigues, J. V.; Waduge, P.; Yamazaki, H.; Cressiot, B.; Chishti, Y.; Makowski, L.; Yu, D.; Shakhnovich, E.; Zhao, Q.; Wanunu, M. Differential Enzyme Flexibility Probed Using Solid-State Nanopores. *ACS Nano* **2018**, *12*, 4494−4502.

(78) Freedman, K. J.; Jürgens, M.; Prabhu, A.; Ahn, C. W.; Jemth, P.; Edel, J. B.; Kim, M. J. Chemical, Thermal, and Electric Field Induced Unfolding of Single Protein Molecules Studied Using Nanopores. *Anal. Chem.* **2011**, *83*, 5137−5144.

(79) Wilson, J.; Sarthak, K.; Si, W.; Gao, L.; Aksimentiev, A. Rapid and Accurate Determination of Nanopore Ionic Current Using a Steric Exclusion Model. *ACS Sens.* **2019**, *4*, 634−644.

(80) Kammann, M.; Laufs, J.; Schell, J.; Gronenborn, B. Rapid Insertional Mutagenesis of DNA by Polymerase Chain Reaction (PCR). *Nucleic Acids Res.* **1989**, *17*, 5404.